ATMOSPHERIC ENVIRONMENT: X 31 (2026) 100487

Contents lists available at ScienceDirect

Atmospheric Environment: X

journal homepage: www.journals.elsevier.com/atmospheric-environment-x

Aerosol dispersion of state-of-art ventilation concepts in passenger trains—A comparative study

Michael Mommert *, André Volkmann, Felix Werner, Daniel Schmeling

Institute of Aerodynamics and Flow Technology, German Aerospace Center (DLR), Bunsenstr. 10, 37073, Goettingen, Germany

ARTICLE INFO

Keywords:
HVAC
Passenger train
Aerosol dispersion
Ventilation

ABSTRACT

We report on an experimental study regarding the performance of state-of-the-art ventilation systems with different inlet positions with respect to the aerosol spread. For that, the spatial distribution of aerosol exposure was determined for six different source locations in a generic passenger compartment. This allowed us to evaluate the different concepts in terms of parameters such as contaminant removal efficiency, the number of seats above a certain threshold or the mean particle concentration in the breathing zone of the passengers. The results revealed strong differences in the local particle concentrations depending on the source position. Further, it was found that two ceiling-based concepts, microjet ceiling and ceiling mounted slot diffusers aimed at the passengers, have significant advantages over the other concepts, especially when it comes to the number of seats with aerosol exposures above certain thresholds. Yet, which concept is optimal still depends on the chosen threshold. The contaminant removal efficiency fluctuates only weakly around 0.5 for the different concepts, revealing mixing-ventilation principles for all concepts.

1. Introduction

Passengers of public transport are exposed to various sources of polluted air during their journeys. These range from emissions of propulsion systems (Liu et al., 2019) to brake or wheel friction emissions (Tu and Olofsson, 2024). With the SARS-CoV-2 pandemic, the exposure to potentially pathogen-carrying air inside the passenger compartments significantly increased in relevance. The ventilation of passenger train compartments has to meet several standards, e.g. EN 13129:2016 for long-distance trains or EN 14750:2024 for urban, suburban and regional rolling stock, to ensure passenger thermal comfort. At the same time, the energy requirements of the HVAC system and the local air quality must be considered. Balancing these three main pillars (thermal comfort, energy demand and air quality) is a challenging task in terms of ventilating passenger trains. Additional constraints are imposed by the geometric and specific operating conditions of the train. Although the air quality in terms of a sufficient fresh air supply has long been defined and stipulated in standards, the aforementioned SARS-CoV-2 pandemic has drawn additional attention to this issue. According to the World Health Organization (WHO) (2021), it has been well accepted since summer 2020 that – besides smear infection and large droplets – aerosols that are absorbed through the mucous membranes of the respiratory tract play a major role in the spread of the virus. This led to an intensification of research into transmission routes and locations, of which public transport became one focus area (Gartland et al., 2022). One branch of this research focuses on modeling transmission ways to estimate infection risks. Examples of such studies can be found for buses (Fouckhardt et al., 2026), airplanes (Webner et al., 2024), and trains (Li et al., 2022).

Further research gave attention to the various factors which can be modified to influence the spread of viruses. Most studies approach this topic with a computational fluid dynamics (CFD) approach, which entails Lagrangian particle transport. As an example, Wang et al. (2014) compare the efficiency of aerosol removal for three different compartment types common in Chinese rail transport. Other studies in a German long-distance train (ICE) segment using computational fluid dynamics simulations (Konstantinov et al., 2023) underlined the positive effect of wearing a mask and the increased particle loads during coughing. Also, various aspects like the specific means of the aerosol emission, i.e. speaking, coughing, or sneezing, have been studied numerically by Wu et al. (2024). On the other hand, Xu et al. (2022) investigate the influence of the particle size on the transport of evaporating particles.

However, simulating a whole train compartment is typically only feasible with a steady-state approach. Whereas, experimental studies showed that local contaminant concentration can strongly fluctuate over time (Schiepel et al., 2025), which indicates a significant impact of transient effects on the particle transport. For this reason, experimental investigations are indispensable when it comes to investigating aerosol

* Corresponding author.
E-mail address: michael.mommert@dlr.de (M. Mommert).

https://doi.org/10.1016/j.aeaoa.2026.100487
Received 7 May 2026; Received in revised form 9 July 2026; Accepted 13 July 2026
Available online 17 July 2026

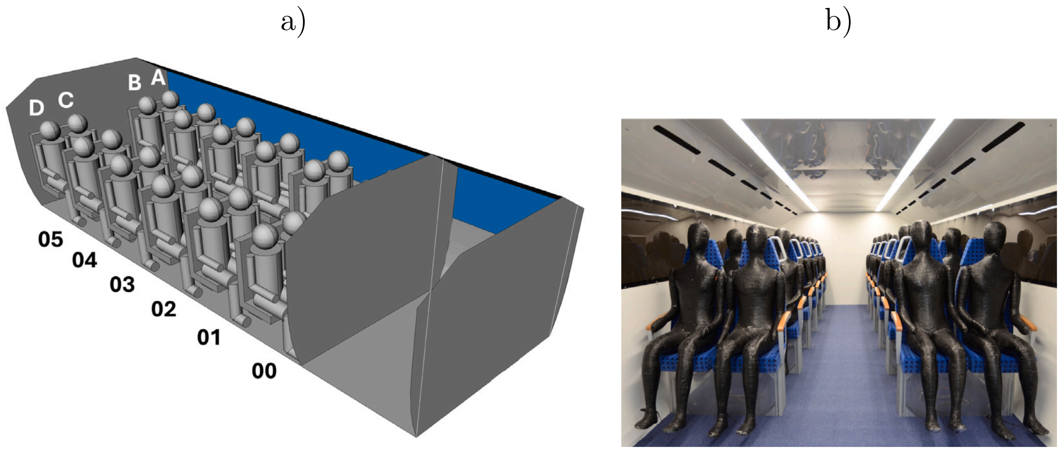

Fig. 1. (a) CAD rendering of the GZG mock-up. (b) Photograph of the mock-up without further installations.

dispersions. The aspects of aerosol dispersion covered by experimental studies cover the effect of mask-wearing and the rate of the fresh-air supply, which was measured in the compartment of a former German long-distance train by Schmeling et al. (2022). The approach used for these investigations, as well as for the presented study, is positioning a realistic face mask with constant aerosol exhalation on a thermal manikin to simulate an index person, while measuring the aerosol dispersion with an array of particulate matter sensors. This approach is well established and has also been used for similar studies in full-size aircraft cabins to investigate the influence of masks and ventilation rates (Schmeling et al., 2023) or different ventilation concepts (Dehne and Schmeling, 2025).

As dedicated measures reacting on pandemic threats, such as mask mandates or the implementation of air purifiers, are both accompanied by social and economic drawbacks, the stock ventilation systems of future train models should be designed as resilient as possible. This reduces the need for dedicated measures in pandemic situations, and mitigates the spread of airborne diseases in general.

With the aim of determining resilient concepts, the main contribution of the present study is the investigation of the aerosol dispersion characteristics of five commonly used supply air inlet concepts, combined with a prescribed outlet type. This complements other studies with different focuses: Schiepel et al. (2025) experimentally investigated different outlet positions, specifically top or bottom, for micro-jet ceiling vents as inlets. These options were further compared with a cabin displacement ventilation concept. Among others, they concluded that the sole change of the exhaust air position from ceiling-based exhaust to floor-based exhaust has only a minor influence on the mean particle load in the breathing zone of the seated passengers. Songbo et al. (2025) present a numerical investigation of the influence of the ratio between top and bottom exhaust utilization. This study also shows that different indicators may point to different optimal solutions.

2. Experimental setup

The following subsection introduces the Generic Train Laboratory (GZG), displayed in Fig. 1, which is used as a mock-up test environment. This section further presents the aerosol generator and the respective particle sensor system.

2.1. Generic train laboratory

The tests were carried out in a generic train laboratory, representing the lower deck of a double-deck high-speed train, ensuring high repeatability and a more general knowledge compared to highly specific solutions for selected train series. The full-scale mock-up consists of 24 seats and a precisely controllable, stationary HVAC unit. Thermal passenger manikins are used for a realistic simulation of the obstruction and heat dissipation of the human passengers. Their heat emission was set to 85 W in reference to the specifications of the standard EN 13129:2016.

For all cases, the supply air flow rate was set to $9.6\ \mathrm{l/s/seat}$, which is similar to the specific supply flow rate of an ICE train carriage (Schmeling et al., 2022), and distributed equally between the 6 or 12 inlet elements. This results in an air exchange rate of approximately $27\ \mathrm{h}^{-1}$. The respective supply air temperatures ranged between 14 °C and 16 °C to achieve the mean interior temperature (definition according to EN 13129:2016) of 23 ± 0.5 °C.

As outlets, two perforated opening elements were installed per row and side of the aisle. They comprise ducting to the surroundings of the mock-up, without any recirculation, meaning that all cases were conducted with a supply of 100% fresh air. While a ventilation without recirculation is atypical for passenger trains, this simplification is justified by recent studies (Schmeling and Shishkin, 2025) showing that the direct transmission path clearly dominates.

2.2. Aerosol generator

A system of aerosol exhalation (made of artificial saliva mixed according to NRF 7.5 (ABDA – Bundesvereinigung Deutscher Apothekerverbände e. V., 1986)) and local particulate matter probes in the breathing zones of all other passenger thermal manikins is used to evaluate the particle spread. The aerosol generator consists of an airbrush pistol (AFC-101 A, nozzle diameter 0.35 mm), pressurized at 2 bar. It is connected to a settling chamber and a facial mask to release the particles through the nose and mouth at a realistic exhalation airflow rate of $12\ \mathrm{l/min}$. The facial mask is attached to the head of one of the thermal passenger manikins, which simulates the index passenger, see Fig. 2. The generated artificial saliva aerosol particle size distribution was in a range below 2.5 μm in diameter and with a peak at 0.8 μm. Thus, the particle size distribution corresponded to a normal breathing scenario (Gupta et al., 2010). The output concentration of the described aerosol source amounts to $c_{\mathrm{source}} = 3 \times 10^5\ \mathrm{cm}^{-3}$, i.e., a generation of 6×10^7 particles per second.

2.3. Sensor system

Local particulate matter sensors are installed in the breathing zones of all other thermal passenger manikins, see orange frame in Fig. 2, as well as in the outlets for the stale air. These sensors are of the type Sensirion SPS30, which measure the relevant concentrations of the range 0.3…2.5 μm directly from the scattered laser light, retrieved by a photo diode. These sensors are factory-calibrated against optical particle sizers (Sensirion AG, 2020). Further, their accuracy has been

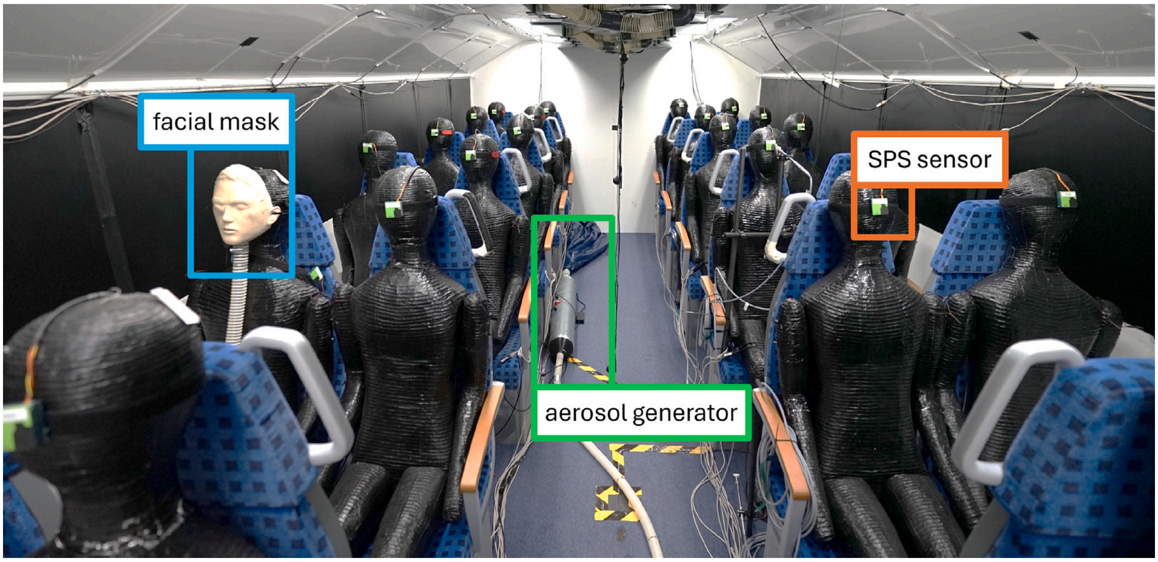

Fig. 2. Interior view of the mock-up with both aerosol source (highlighted with green and blue frames) and sensor system (single sensor highlighted with orange frame) installed.

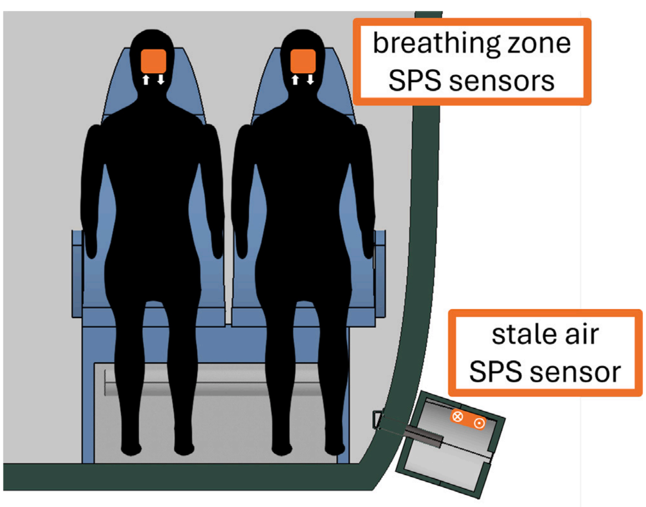

Fig. 3. Vertical section showing two instrumented thermal manikins and one instrumented outlet element with a settling chamber on the exterior side of the mock-up. The white arrows indicate the inflow and outflow of the sensors.

confirmed against an optical particle sizer (TSI OPS 3330) by Schiepel et al. (2022). This study found the accuracy of the sensors within ±5% of the reference instrument for the relevant concentration range below 2500 cm^{-3}. Moreover, Fig. 3 shows how the assembly recommendations (Sensirion AG, 2019) by the manufacturer were taken into account: The sensors were mounted so that the its outlet opening faces downwards or lies below the inlet in order to minimize dust accumulation. In order to insulate them from the heated manikins, the sensors were mounted with hook-and-loop fasteners. The stale air sensors were mounted within settling chambers, so that they are not directly exposed to the exhaust flow.

A data acquisition system (Niehaus and Westhoff, 2022) allows for a simultaneous operation of all sensors with a recording frequency of approx. 0.9 Hz. The same measurement system has been used in other train and aircraft cabins and more information can be found in Schmeling et al. (2022, 2023). Evaluated number concentration values are normalized to the source strength and given in permille (‰).

3. Methodology

3.1. Investigated cases

We investigate a variety of air supply concepts, compared for a common outlet concept. Concretely, longitudinal openings along the lower edges were used as outlets. An overview and schematics of the investigated configurations is summarized in Table 1. For the case Sc1, twelve slot diffusers were installed below the ceiling with the adjustable slot set up in a way that the supply air is ejected directly towards the seated manikins, while they are heated. A laser visualization of the flow arrangement, as well as an image of the setup of this and the other cases, can be found in Appendix A. The above-mentioned slot diffusers were also used for the cases Sc3, Sc4, and Sc5. For Sc3, they were mounted the same way as for Sc1, but with the slots adjusted to produce horizontal supply air jets. In contrast, the diffusors were mounted both below or and above the windows for Sc4 and Sc5, respectively. In both of these configurations, the slots were adjusted for vertical supply air jets. For the investigation for Sc2, six micro-jet elements were installed as ceiling vents above the aisle.

3.2. Test procedure

For the investigation of the different concepts, each one was tested for six different source positions, specified as seat numbers referring to Fig. 1(a): C01, D01, C03, D03, C05, and D05. This restriction to one side of the aisle represents a trade-off between measurement expenditures and the consideration of a broad range of source placements within the compartment, i.e. aisle/window and front/center/back, by also taking its symmetry into account.

Fig. 4 shows the timeseries of the aerosol concentration c of an exemplary source (D01) and sensor (D02) location for the different cases. It illustrates how the tests were carried out for each case and each source location: The source is started at $t = 0$ s, leading to an increase in aerosol concentration within the compartment. The various concentrations stop to rise and level out after about 600 s. As the displayed time series then still exhibit significant fluctuations of up to 100 cm^{-3} in amplitude in the measured concentrations, for the example of a sensor in the vicinity (D02) of the source (D01), the investigations below are based on time averaged values taken over the last 300 s before the source is switched off after at least 1200 s. This interval is highlighted by the two dashed lines in Fig. 4. After the shutdown of the

Table 1
Investigated generic concepts of a cooling air supply for a common outlet solution.

	inlet				
outlet	Sc1	Sc2	Sc3	Sc4	Sc5
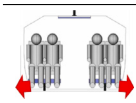	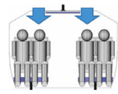	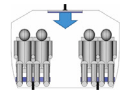	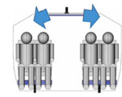	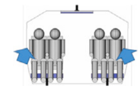	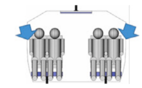

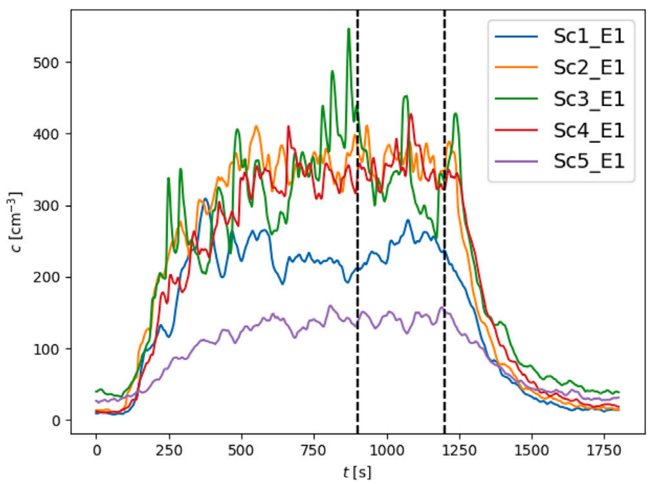

Fig. 4. Timeseries of the aerosol concentration of particles between 0.3 μm and 2.5 μm for the various cases. The timeseries shown refer to the exemplary sensor location D02, while the source is positioned at D01. The dashed lines indicate the averaging time interval of 300 s, just before the source is switched off.

source, an exponential decline of the aerosol concentration is observed. This phase takes about 600 s before the concentrations level off again and the next test can be started.

The timeseries displayed in Fig. 4 also show significant differences of the exposure levels for the source-sensor combination D01–D02 with most of the cases averaging at about 350 cm^{-3}, while Sc1 and Sc5 exhibit significantly lower exposure levels of approximately 250 cm^{-3} and 150 cm^{-3}, respectively. Such single source-sensor combinations are, however, highly incomplete when it comes to evaluating ventilation concepts regarding aerosol dispersion.

Therefore, concentration maps based on the described time averages are generated for each source location. These maps are shown in Fig. 5 for the example of case Sc1. For a more intuitive understanding, the fraction of aerosol concentration with respect to the source concentration $f_N = \frac{c}{c_{\text{source}}}$ is used from here on. In these maps, the colored rectangles represent the aerosol levels of the respective seats while the arrows represent the aerosol levels of the respective exhaust lines. The overview of the six maps allows to understand detailed characteristics of the ventilation concepts. For the given example of Sc1, the longitudinal dispersion is the weakest for the central source locations C03 and D03. In contrast, the longitudinal dispersion is strongly pronounced towards the front of the compartment for the source positions C01 and D01. The source positions in the back of the compartment are distinguished by a strong cross-aisle dispersion. This effect is less prominent the further the source is located towards the front of the compartment. For the central position, with moderate cross-aisle contamination, the location of the highest cross-aisle aerosol level is also shifted towards the front. Complete maps of all other cases can be found in Appendix B. This allows the study to remain concise while providing insight into the details of each case. A very brief discussion of the other ventilation concepts as depicted in Appendix B reveals for all concepts a strong dispersion of exhaled particles on the other side of the aisle if the source is located in the last row. Especially for the concepts Sc3-Sc5 rather high aerosol fractions were found on the whole rear row. Furthermore, it was observed that the highest contaminated seat is almost always in the direct neighborhood of the source, their absolute values, however, deviate strongly. The individual spreading maps reveal for all concepts that there is only a marginal difference of the spreading if the source moves within the same row from the aisle (C) to the window seat (D). Only at the case Sc5 and the middle row the change from aisle to window seat resulted in a change of the overall spreading pattern: mainly forward from the aisle seat (C03) and homogeneious distributed for the window seat (D03) with even higher concentrations in the adjacent rearward outlet (CD, row 04) compared to the forward outlets. In order to provide a more concise yet spatially resolved overview, a further investigation step involves the averaging of all six maps. These average maps are part of the comparison between the different cases in Section 4 which also discusses the following performance indicators.

3.3. Performance indicators

Mean and maximum aerosol concentrations. These parameters represent the respective particle concentration regarding the sensors positioned in the breathing zones of the manikins. The values refer to the time averages discussed in Section 3.2. Both types, mean and maximum, are also averaged over all six source positions investigated per case. Hence, they show the concentrations passengers might inhale on average for an unknown placement (mean) of the index passenger or the respective worst case positioning (maximum).

Contaminant removal efficiency (CRE). This parameter expresses the particle concentration within the exhaust openings in relation to the mean particle concentration within the cabin. Based on the available instrumentation, we use two assumptions:

First, the mean particle concentration of the passenger compartment is represented by the average of the sensors positioned within the breathing zones. While this deviates from the common definition, we argue that a breathing-zone centered CRE is particularly relevant for contaminants affecting respiratory tracts.

Second, the exhaust flow rate is distributed homogeneously over the exhaust openings, meaning that an average over the sensors represents flow-rate averaged values. This assumption is based on the fact that the outlet and inlet concepts are all installed over the complete length of the compartment with a mirror symmetry towards the vertical longitudinal plane. So, there is no reason to assume a systematic bias towards higher or lower CRE due to exhaust inhomogeneities.

The parameter CRE is defined in the interval between 0 and 1, with 1 representing perfect removal and 0.5 representing perfect mixing. For details see Brouns and Waters (1991).

Seats over threshold. For this metric, generic thresholds of 0.5, 1, and 2 ‰ were defined as possible time-averaged concentrations leading to a critical infection risk. This allows one to compare the concepts in terms of expected infections for generic airborne diseases with stronger (low threshold), moderate, or weaker (high threshold) infectivity. While a translation of these thresholds into concrete infection risks is possible (Webner et al., 2024), they would be strongly dependent on pathogen-specific emission rates, which vary by orders of magnitude between

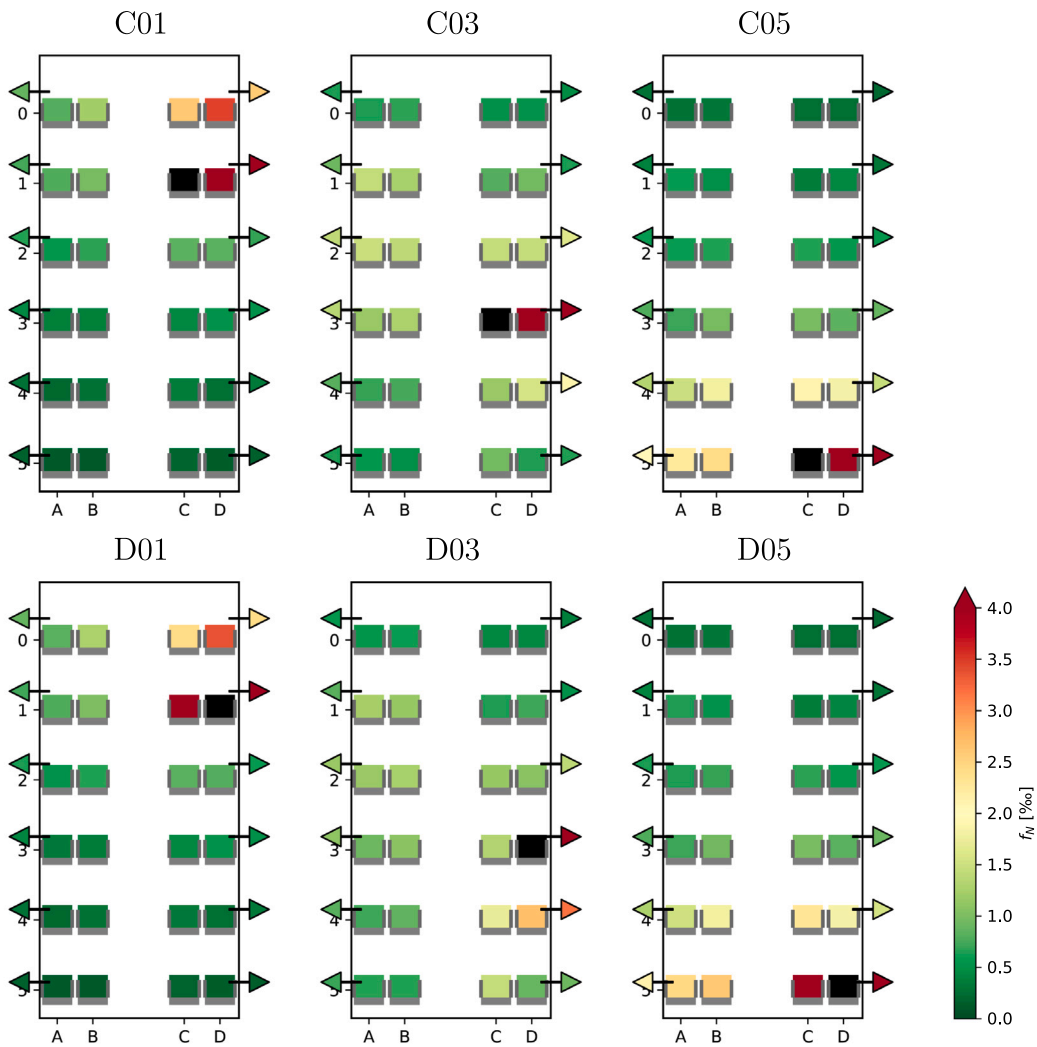

Fig. 5. Maps of the aerosol fraction f_N for all investigated source positions of case Sc1. Color-coded rectangles represent the aerosol levels in the breathing zones of the respective seats. Arrows indicate the aerosol levels in the respective exhausts.

diseases, strains of a virus, or even single studies of one virus type. For that reason, the present study limits its focus to transport-related parameters, highlighting the characteristics of the different concepts.

As for the other indicators, these values are also averages over all source positions, if not stated otherwise.

4. Results and discussion

This section comprises the comparison of the different ventilation concepts, starting with their averaged spreading maps, which are followed by the introduced performance indicators. For the latter, we mainly discuss the averages of the six measurements per concept, which are associated with different source positions. To determine the significance of differences between two concepts, the six measurements are considered as samples of each concept, which are paired, as the same source positions were used for each concept. Thus, the detailed *p*-values, indicating the significance of the following results, can be found in Appendix C.

4.1. Averaged spreading maps

For the comparison of the different cases, we first assess the averages of the aerosol dispersion maps over all six source positions, which are displayed in Fig. 6. Besides the overall concentration levels being discussed in more detail below, these maps specifically express the general cross-aisle contamination towards the A and B seats as well as longitudinal gradients.

Regarding cross-aisle contamination, the cases Sc3 and Sc4 exhibit the effect the strongest, as they show elevated f_N values for the A and B seats over the complete length of the compartment. Of the remaining cases, Sc1 performs the best, with the lowest average aerosol fractions on the A and B seats. Additional to this lateral gradient, all cases show a form of longitudinal gradient with higher values towards the back of the compartment. We attribute this to the fact that the source positions in row 5 typically generate the strongest aerosol spread, as it is observable in Fig. 5 (and in Appendix B).

4.2. Mean and maximum contaminations

In order to determine the global performance metrics, the mean and maximum values of the aerosol fractions are compared by bar charts in Fig. 7. The respective error bars of this and the following charts indicate the standard deviations associated with the averaging over the different source positions.

The comparison of the different cases reveals different trends with regard to the mean and maximum values. Regarding the mean concentration, Sc1 and Sc2 perform best with values of approximately 1 ‰. Compared to that, the other cases perform worse exhibiting higher

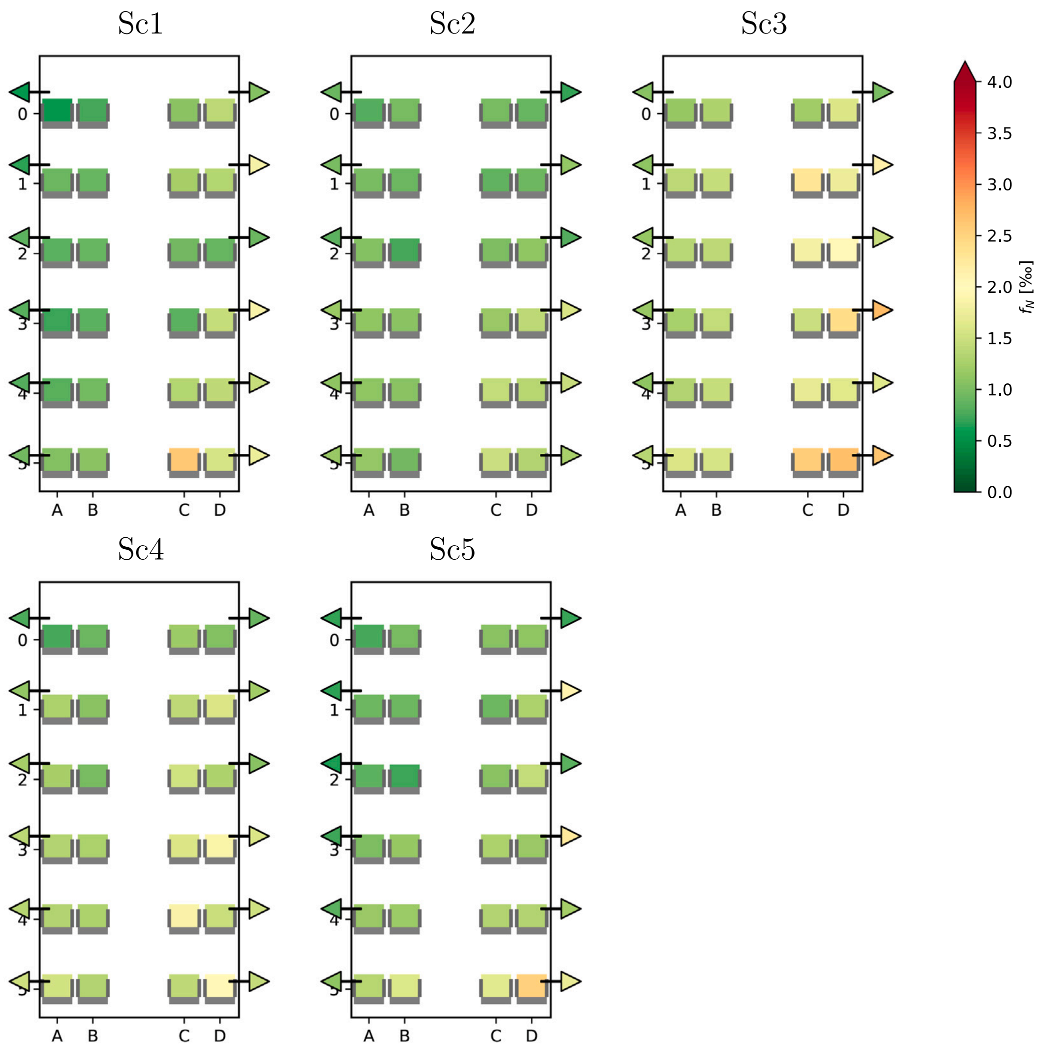

Fig. 6. Maps of the aerosol fraction f_N averaged over all investigated source positions for the different cases. Color-coded rectangles represent the aerosol levels in the breathing zones of the respective seats. Arrows indicate the aerosol levels in the respective exhausts.

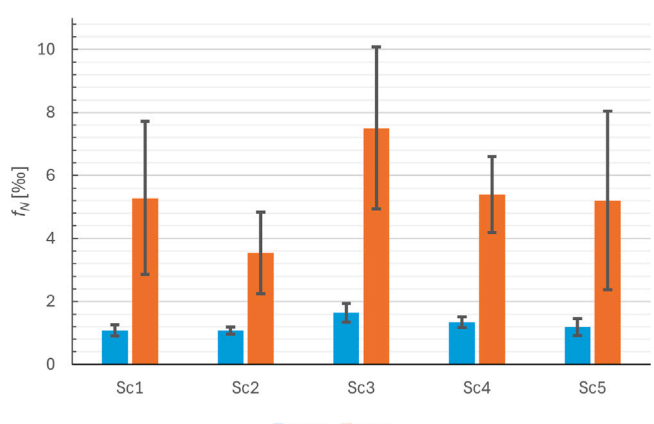

Fig. 7. Source-position averages of the mean (blue) and maximum (orange) aerosol fractions of all seat positions. Error bars represent the standard deviations associated with the different source positions.

values. Significant differences exist towards the configurations Sc4, with 1.3 ‰, and Sc3, with approximately 1.6 ‰.

Regarding the maximum concentration, the standard deviations based on the different source positions amount to significant portions of the displayed values, reaching up to 54% at Sc5. For this reason, Sc1, Sc4, and Sc5 are considered having an equal performance of around 5 ‰. The only concepts displaying significant deviations from other ones are Sc2 and Sc3. For the latter, the deviation is again towards a worse performance with approximately 7.5 ‰. In contrast, Sc2 shows with 3.5 ‰ the best performance regarding the maximum concentration within the compartments breathing zones.

4.3. Contaminant removal efficiency

The next comparison of the cases considers the contaminant removal efficiencies displayed in Fig. 8. The bar chart shows that the CRE values of all cases are closely arranged around 0.5, which is also expected for mixing ventilation concepts.

The small deviations between the cases further follow the trend already observed for the mean concentrations, with Sc1 and Sc2 exhibiting the more favorable values. However, the small overall deviations lead to only Sc2 having a significant advantage over Sc4. This suggests that this indicator is not ideal for evaluating the performance of different ventilation concepts regarding a direct disease transmission path.

4.4. Seat above a threshold

Due to these deficiencies of the CRE, the next comparison is based on the number of seats above certain thresholds, resembling a strongly

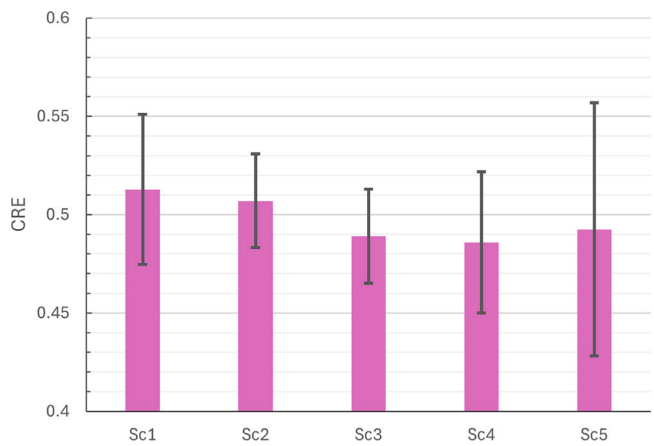

Fig. 8. Source-position averages of the contaminant removal efficiencies (CRE) of the different concepts. Error bars represent the standard deviations associated with the different source positions.

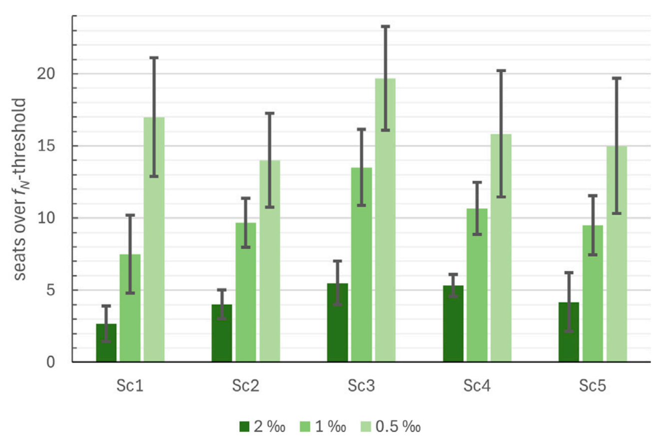

Fig. 9. Source-position averages of the seats above given threshold aerosol fractions. Error bars represent the standard deviations associated with the different source positions.

simplified infection model, where the number of seats exceeding a threshold represents potential infections. These numbers are presented in form of a bar chart in Fig. 9.

It is remarkable that the different thresholds again lead to different results in the comparison of the cases. For the high (2 ‰) and medium (1 ‰) thresholds, the comparison between the cases yields similar results: The best performance is achieved by Sc1 (H: 3 M: 8 seats), which is followed by a midfield comprised by Sc2 and Sc5 (H: 4 M: 10 seats), as well as Sc4 (H: 5 M: 11 seats). The worst results, on the other hand, are produced with Sc3 (H: 6 M: 14 seats). So, while the differences of the CRE between the cases were mostly insignificant, the difference between the best and worst case could mean the number of seats over a threshold doubling. In contrast to the other thresholds, Sc2 (14 seats) performs significantly better for the low (0.5 ‰) threshold than all other concepts except for Sc5, which reaches a similar performance with 15 seats on average. In this category, Sc1 underperforms with an average of 17 seats, only exceeded by the significantly worse performing Sc3 with about 20 seats.

4.5. Discussion and limitations

Summarizing these results, the following key messages are evident: The metric used to compare the concepts matters, as different metrics produced minimal (CRE) or significant (seats over threshold) differences between the different concepts and different ranking orders of concepts. As minimizing pathogen transport is only one aim of designing a ventilation solution besides passenger comfort and energy efficiency, we propose using a metric that is as close as possible to the ultimate goal of reducing infections. This metric could then be weighed against the other goals. Based on the here available experimental data, we consider seats-over-threshold to be closest to the ultimate goal of reducing infections. However, translating the results of this metric into actual infections still depends on the specific application (expected travel time within the compartment), combined with the considered pathogen (infectivity). In these regards, it has to be noted that there is no single optimal ventilation concept. Yet, both Sc1 and Sc2 showed to be advantageous over the different metrics. Considering all metrics, their different characteristics are revealed: The case Sc1, with the inflow aimed directly towards the passengers, exhibits a controlled aerosol transport characteristic in close proximity to the source, while its characteristic is better described by dilution through dispersion in the far field. For case Sc2, with the microjet ceiling, the exact opposite applies. This case shows dilution through dispersion in proximity to the source and a more controlled transport on the larger scales. This explains why Sc1 performs best for the seats above the higher thresholds (see Fig. 9), while Sc2 still shows the lowest number of seats for the 0.5 ‰ threshold and the lowest maximum values (see Fig. 7).

Regarding a transfer to real world applications, the limitations caused by the following simplifying omissions need to be considered: persons walking in the aisle, changes of the occupancy during a travel or partial occupancy, door openings, solar radiation heat loads, and possibly more. However, the supply air flow rate is typically kept constant in a train to avoid temperature inhomogeneities and/or too high flow velocities. Further, due to the rather high flow rates, the large-scale flow structures are mainly determined by the mixing ventilation scheme and only weakly changed by internal heat loads or different boundary conditions. Consequently, we expect that our findings are in general transferable to other geometries and will also be valid for varying other conditions. Yet, local differences of the aerosol dispersion are to be expected. With regard to door openings, one has to distinguish between long-distance trains (less frequent door openings and typically additional separation doors between the passenger seats and the entrance areas) and sub-urban or metro trains (frequent openings and doors directly in the passenger area). While for long-distance trains, a negligible effect of door-openings is expected, the effect should be integrated in further studies on trains operating on shorter distances.

5. Conclusion and outlook

We investigated the aerosol dispersion for five different inlet concepts in a generic passenger compartment of a train by measuring aerosol concentration in the breathing zones and exhaust lines for six different source locations for each case. For the evaluation, the metrics of mean concentration, maximum concentration, contaminant removal efficiency and seats above threshold were considered. While the variance between the cases was low for the contaminant removal efficiency, the spread within the other metrics amounted up to a doubling between best and worst concept. Regarding the performance of the concepts, different metrics resulted in different orders. However, the trend over all metrics revealed that the concept Sc3, sideways oriented ceiling inlets, is disadvantageous regarding the containment of the aerosol spread. In contrast, the concepts Sc1, ceiling inlets oriented towards the passengers, and Sc2, a microjet ceiling, proved to be advantageous for the reduction of the spread of particles.

However, these two concepts exhibit different short range and large scale flow characteristics, which leads to Sc1 being optimal for avoiding infections of pathogens with lower infectivities (associated with higher threshold concentrations) and Sc2 being optimal for the highest infectivity (associated with the lowest threshold concentration).

Additionally, the investigation revealed trends overarching all concepts, such as a longitudinal draft towards the front of the compartment, as well as stronger cross-aisle contamination for source positions at the very back of the compartment.

Even under consideration of the discussed limitations, the presented results may indicate which concepts should be preferably pursued or avoided during the development of novel passenger trains. While this indication is justified by concept-specific, large-scale flow structures forming largely independent of specific train geometries, studies of the application in concrete geometries are certainly still necessary to quantify the respective dispersion characteristics.

Besides state-of-the-art concepts, upcoming research focuses on inhibiting the spread of pathogens through developing air supply concepts tailored for this very purpose. Further, the application of more elaborate infection models, like the one presented by Webner et al. (2024), should also be extended towards experimental investigations, as expected infections are the relevant metric. The necessary information for modeling the particle age may be gathered by analyzing the exponential responses of switching the source on or off.

CRediT authorship contribution statement

Michael Mommert: Writing – original draft, Visualization, Methodology, Investigation, Formal analysis, Data curation, Conceptualization. **André Volkmann:** Resources, Investigation, Data curation. **Felix Werner:** Resources, Investigation, Data curation. **Daniel Schmeling:** Writing – review & editing, Supervision, Project administration, Methodology, Funding acquisition, Conceptualization.

Declaration of Generative AI and AI-assisted technologies in the writing process

During the preparation of this work the author(s) used DeepL in order to conduct language editing. After using this tool/service, the author(s) reviewed and edited the content as needed and take(s) full responsibility for the content of the publication.

Declaration of competing interest

The authors declare that they have no known competing financial interests or personal relationships that could have appeared to influence the work reported in this paper.

Acknowledgments

Funded by the European Union. Views and opinion expressed are however those of the author(s) only and do not necessarily reflect those of the European Union or the Europe's Rail Joint Undertaking. Neither the European Union nor the granting authority can be held responsible for them. The project FP4-Rail4EARTH is supported by the Europe's Rail Joint Undertaking and its members.

Appendix A. Laser visualization of ventilation concepts

This appendix provides a more detailed view of the technical implementation of the investigated inlet concepts. Smoke visualizations in a cross-section of the compartment further supplement the understanding of the resulting flow.

A.1. Case Sc1

The concept Sc1 comprised the installation of slot-diffuser inlets under the ceiling. The vanes of the diffuser elements were adjusted in a manner, that the air flow is directed towards the center of the two seat groups on each side of the aisle. The result is displayed in Fig. A.10.

A.2. Case Sc2

For this configuration, micro-jet ceiling elements were installed in the mock-up. As shown in Fig. A.11, this resulted in a down-welling large-scale circulation within the aisle region.

A.3. Case Sc3

For the concept Sc3, shown in Fig. A.12, the slot diffusers were mounted in the same way as for Sc1. However, the vanes are now adjusted so that the air enters the cabin with a horizontal momentum, subsequently following the contour of the ceiling. Respectively, the configuration induces a large-scale circulation with up-welling air in the aisle region.

A.4. Case Sc4

The concept Sc4 represents supply air openings in the lower window sills facing upwards. Hence the slot diffusers were mounted below the window region. The resulting flow displayed in Fig. A.13 follows the side wall/window contour of the compartment to the ceiling; there, it converges, yielding a down-welling flow in the aisle region.

A.5. Case Sc5

In contrast to the concept Sc4, Sc5 represents an air supply through the upper window frame directed downwards. Accordingly, the slot diffusers are mounted as shown in Fig. A.14. The resulting large-scale circulation exhibits an up-welling flow in the aisle.

Appendix B. Time-averaged aerosol concentration for each source position

This appendix provides the dispersion maps for each inlet configuration and source position.

B.1. Case Sc1

For the detailed dispersion maps of case Sc1, see Fig. 6 in Section 3.2.

B.2. Case Sc2

See Fig. B.15.

B.3. Case Sc3

See Fig. B.16.

B.4. Case Sc4

See Fig. B.17.

B.5. Case Sc5

See Fig. B.18.

a) b)

Fig. A.10. (a) Detail image of the vane setting of the slot diffusers. (b) Laser-smoke visualization of the inflow provided by concept Sc1.

a) b)

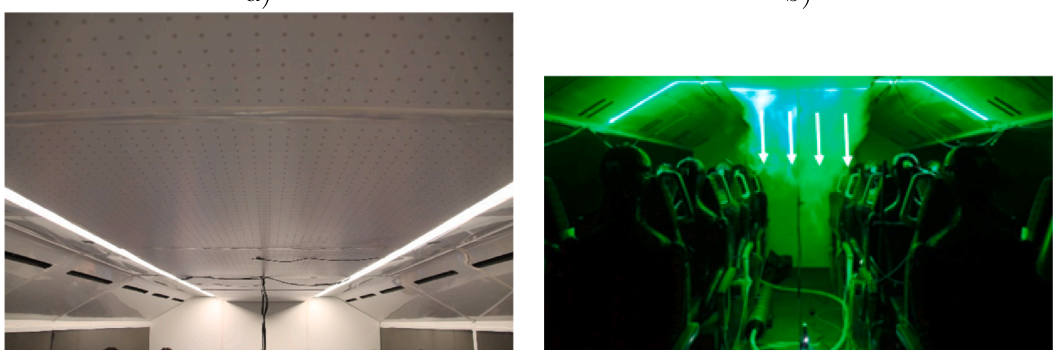

Fig. A.11. (a) Microjet ceiling elements used as supply air inlet in this case. (b) Laser-smoke visualization of the inflow provided by concept Sc2.

a) b)

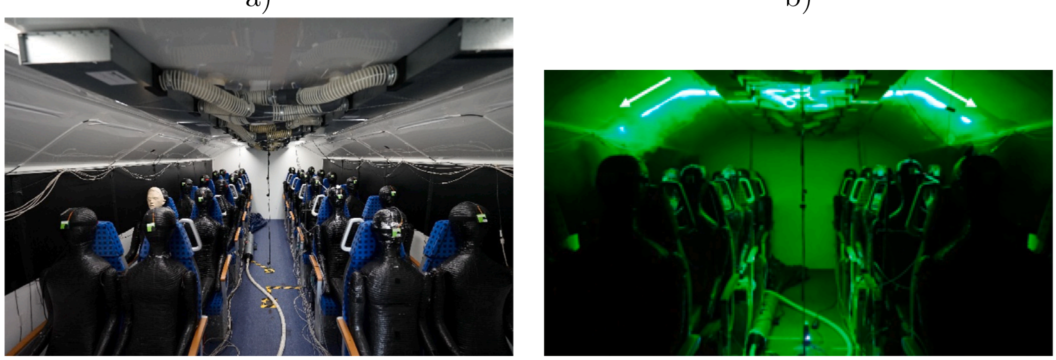

Fig. A.12. (a) Slot diffusers as supply air inlets mounted below the ceiling (as also for Sc1). (b) Laser-smoke visualization of the inflow provided by concept Sc3.

a) b)

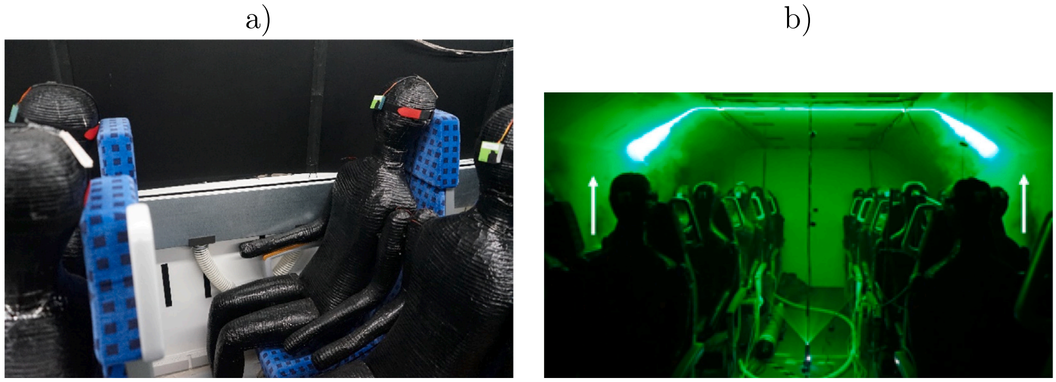

Fig. A.13. (a) Slot diffusers mounted below the window region as inlets for the concept Sc4. (b) Laser-smoke visualization of the inflow provided by concept Sc4.

Fig. A.14. (a) Slot diffusers mounted above the window region as inlets for the concept Sc5. (b) Laser-smoke visualization of the inflow provided by concept Sc5.

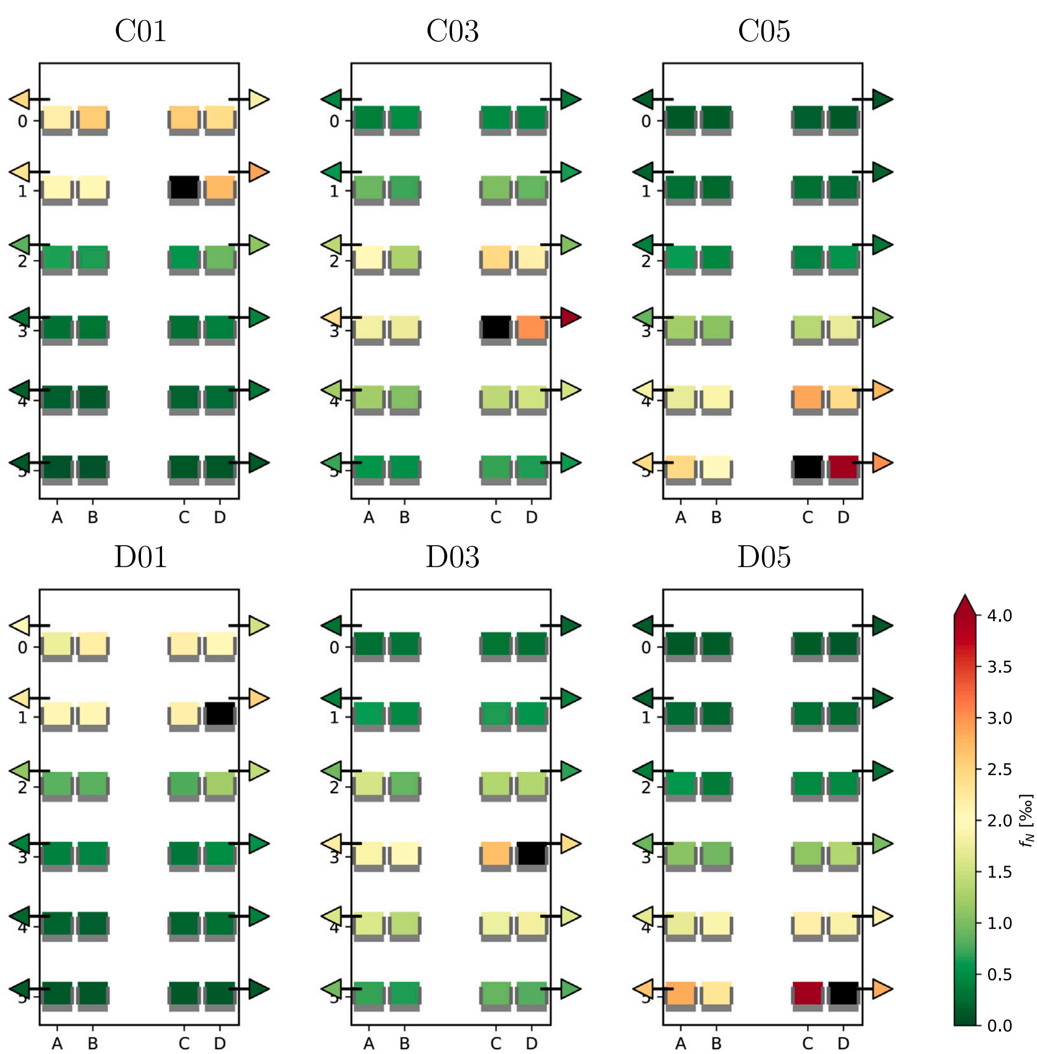

Fig. B.15. Maps of the aerosol fraction f_N for all investigated source positions of case Sc2. Color-coded rectangles represent the aerosol levels in the breathing zones of the respective seats. Arrows indicate the aerosol levels in the respective exhausts.

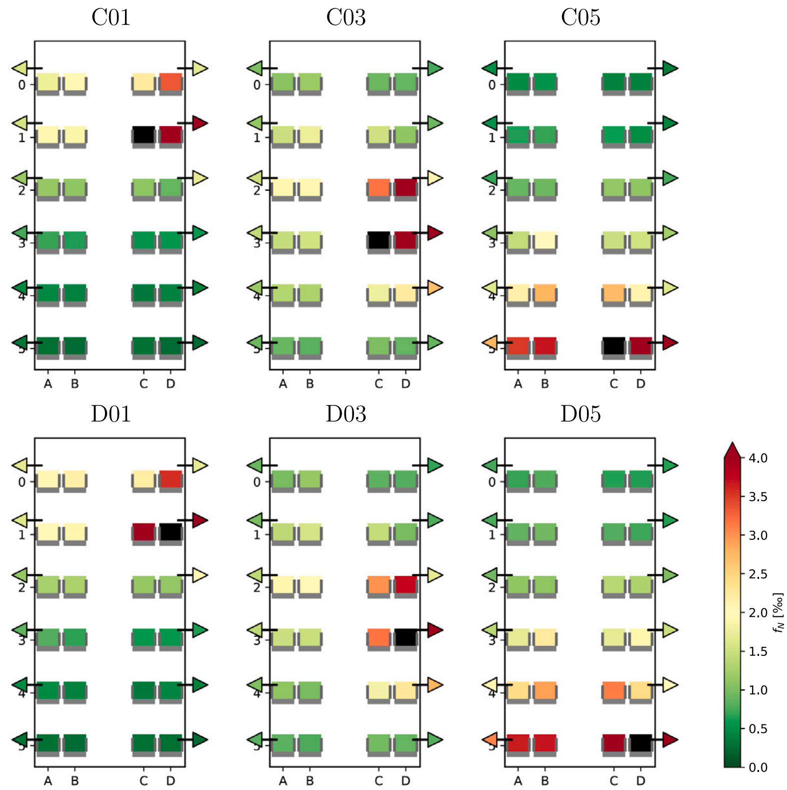

Fig. B.16. Maps of the aerosol fraction f_N for all investigated source positions of case Sc3. Color-coded rectangles represent the aerosol levels in the breathing zones of the respective seats. Arrows indicate the aerosol levels in the respective exhausts.

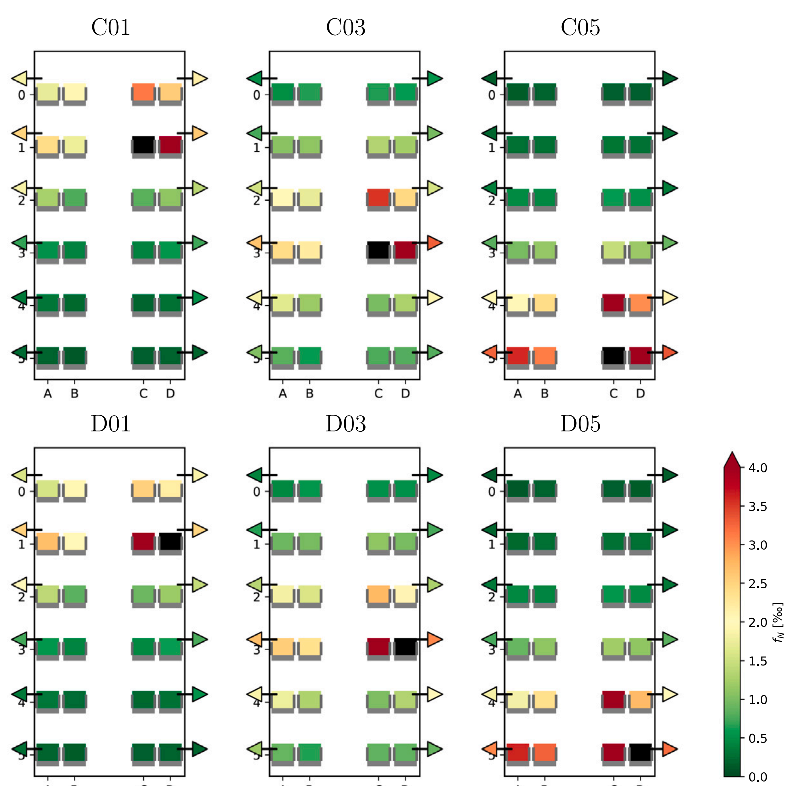

Fig. B.17. Maps of the aerosol fraction f_N for all investigated source positions of case Sc4. Color-coded rectangles represent the aerosol levels in the breathing zones of the respective seats. Arrows indicate the aerosol levels in the respective exhausts.

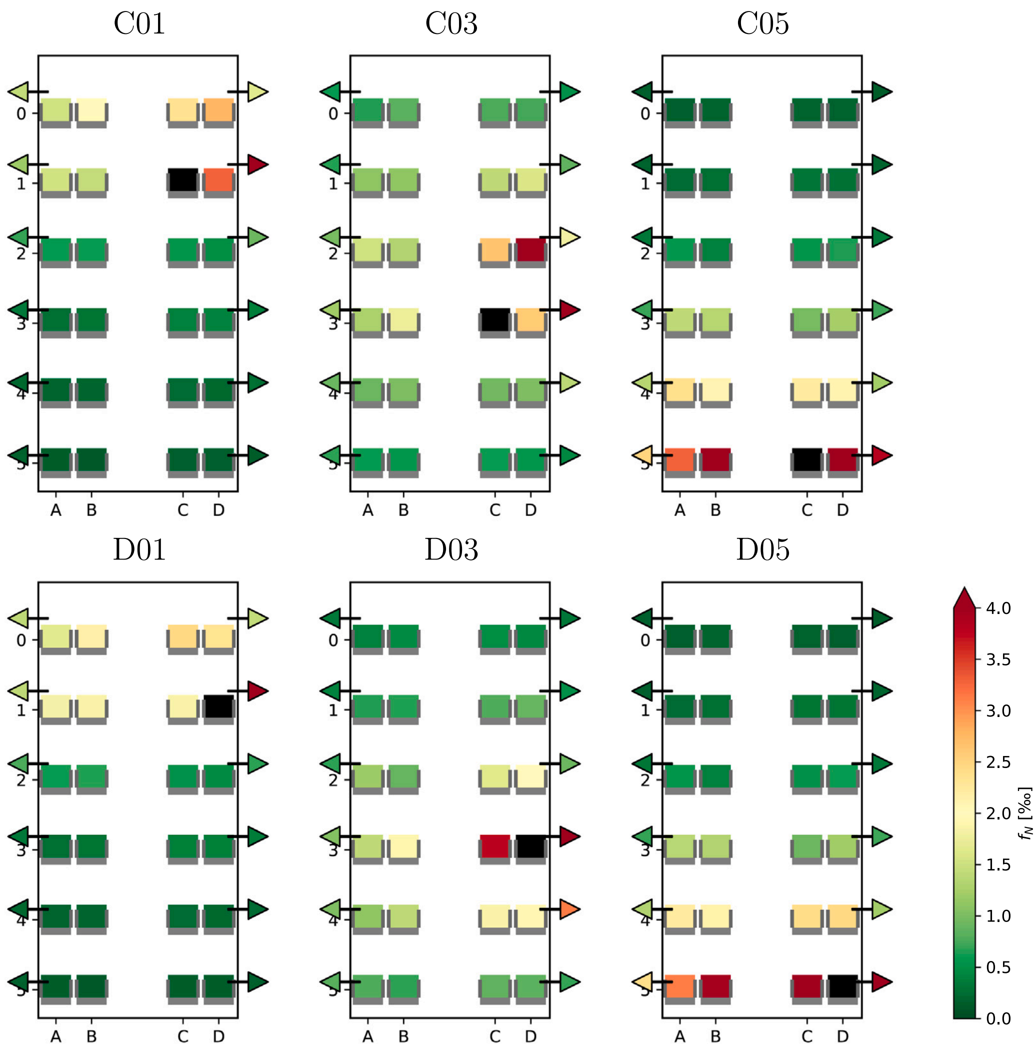

Fig. B.18. Maps of the aerosol fraction f_N for all investigated source positions of case Sc5. Color-coded rectangles represent the aerosol levels in the breathing zones of the respective seats. Arrows indicate the aerosol levels in the respective exhausts.

Appendix C. Significance analysis

To assess the significance of the differences between the concepts, p-values are calculated based on paired-sample, two-tailed t-tests, as the same source positions are sampled for each ventilation concept, and listed in tables for each investigated performance indicator. The p-value entries are rounded to the third decimal place. The cell shading indicates significance levels: ▪ $p \leq 0.05$, ▪ $p \leq 0.01$, ▪ $p \leq 0.001$.

C.1. Mean and maximum aerosol concentrations

The following tables comprise p-values indicating the significance of the difference between all combinations of two concepts, regarding their mean (Table C.2) and maximum concentrations (Table C.3), as shown in Fig. 7.

C.2. Contaminant removal efficiency

The following table comprises p-values indicating the significance of the difference between all combinations of two concepts, regarding their CRE values (Table C.4), as shown in Fig. 8.

Table C.2
p-values indicating the significance of the differences between two concepts regarding their mean aerosol concentrations.

	Sc1	Sc2	Sc3	Sc4	Sc5
Sc1	–				
Sc2	0.843	–			
Sc3	0.000	0.001	–		
Sc4	0.012	0.000	0.021	–	
Sc5	0.190	0.169	0.001	0.052	–

Table C.3
p-values indicating the significance of the differences between two concepts regarding their maximum aerosol concentrations.

	Sc1	Sc2	Sc3	Sc4	Sc5
Sc1	–				
Sc2	0.038	–			
Sc3	0.033	0.003	–		
Sc4	0.927	0.016	0.062	–	
Sc5	0.951	0.113	0.030	0.833	–

Table C.4
p-values indicating the significance of the differences between two concepts regarding their CRE values.

	Sc1	Sc2	Sc3	Sc4	Sc5
Sc1	–				
Sc2	0.694	–			
Sc3	0.118	0.087	–		
Sc4	0.080	0.042	0.706	–	
Sc5	0.346	0.523	0.871	0.642	–

Table C.5
p-values indicating the significance of the differences between two concepts regarding their seats over the 2 ‰ threshold.

	Sc1	Sc2	Sc3	Sc4	Sc5
Sc1	–				
Sc2	0.025	–			
Sc3	0.002	0.107	–		
Sc4	0.007	0.062	0.771	–	
Sc5	0.045	0.842	0.025	0.180	–

Table C.6
p-values indicating the significance of the differences between two concepts regarding their seats over the 1 ‰ threshold.

	Sc1	Sc2	Sc3	Sc4	Sc5
Sc1	–				
Sc2	0.034	–			
Sc3	0.000	0.001	–		
Sc4	0.002	0.111	0.005	–	
Sc5	0.025	0.611	0.000	0.034	–

Table C.7
p-values indicating the significance of the differences between two concepts regarding their seats over the 0.5 ‰ threshold.

	Sc1	Sc2	Sc3	Sc4	Sc5
Sc1	–				
Sc2	0.007	–			
Sc3	0.021	0.004	–		
Sc4	0.341	0.038	0.064	–	
Sc5	0.007	0.253	0.011	0.434	–

C.3. Seats over threshold

The following tables comprise *p*-values indicating the significance of the difference between all combinations of two concepts, regarding their number of seats over the high (Table C.5), medium (Table C.6), and low thresholds (Table C.7), as shown in Fig. 9.

Data availability

Data will be made available on request.

References

ABDA – Bundesvereinigung Deutscher Apothekerverbände e. V. (Ed.), 1986. Deutscher Arzneimittel-Codex, Neues Rezeptur-Formularium. Avoxa - Mediengruppe Deutscher Apotheker GmbH, Eschborn, ISBN: 978-3-7741-0044-2, https://d-nb.info/1049995430.

Brouns, C., Waters, B., 1991. A Guide to Contaminant Removal Effectiveness. Technical Report TN 28.2, Air Infiltration and Ventilation Centre, https://www.aivc.org/resource/tn-282-guide-contaminant-removal-effectiveness.

Dehne, T., Schmeling, D., 2025. Influence of seating position and ventilation on aerosol dispersion in a passenger aircraft. CEAS Aeronaut. J. http://dx.doi.org/10.1007/s13272-025-00915-1.

EN 13129:2016, Railway application - Air conditioning for main line rolling stock - Comfort parameters and type tests.

EN 14750:2024, Railway applications - Air conditioning for urban, suburban and regional rolling stock - Comfort parameters and type tests.

Fouckhardt, L., Sommer, C., Schneider, N., 2026. Modeling the infection risk in vehicles of local public transport for aerosol transmitted viruses. J. Transp. Health 49, 102285. http://dx.doi.org/10.1016/j.jth.2026.102285.

Gartland, N., Fishwick, D., Coleman, A., Davies, K., Hartwig, A., Johnson, S., van Tongeren, M., 2022. Transmission and control of SARS-CoV-2 on ground public transport: A rapid review of the literature up to May 2021. J. Transp. Health 26, 101356. http://dx.doi.org/10.1016/j.jth.2022.101356.

Gupta, J.K., Lin, C.-H., Chen, Q., 2010. Characterizing exhaled airflow from breathing and talking. Indoor Air 20 (1), 31–39. http://dx.doi.org/10.1111/j.1600-0668.2009.00623.x.

Konstantinov, M., Schmeling, D., Wagner, C., 2023. Numerical simulation of the aerosol formation and spreading in an air-conditioned train compartment. J. Aerosol Sci. 170, 106139. http://dx.doi.org/10.1016/j.jaerosci.2023.106139.

Li, T., Wu, S., Yi, C., Zhang, J., Zhang, W., 2022. Diffusion characteristics and risk assessment of respiratory pollutants in high-speed train carriages. J. Wind Eng. Ind. Aerodyn. 222, 104930. http://dx.doi.org/10.1016/j.jweia.2022.104930.

Liu, Q., Hallquist, Å.M., Fallgren, H., Jerksjö, M., Jutterström, S., Salberg, H., Hallquist, M., Le Breton, M., Pei, X., Pathak, R.K., Liu, T., Lee, B., Chan, C.K., 2019. Roadside assessment of a modern city bus fleet: Gaseous and particle emissions. Atmospheric Environ.: X 3, 100044. http://dx.doi.org/10.1016/j.aeaoa.2019.100044.

Niehaus, K., Westhoff, A., 2022. An open-source data acquisition system for laboratory and industrial scale applications. Meas. Sci. Technol. 34 (2), 027001. http://dx.doi.org/10.1088/1361-6501/ac9994.

Schiepel, D., Brinkema, R., Schmeling, D., 2022. Artificial saliva aerosol source and detection system for spreading analysis in indoor environments. In: 17th International Conference on Indoor Air Quality and Climate, INDOOR AIR 2022. https://elib.dlr.de/148451/.

Schiepel, D., Volkmann, A., Schmeling, D., 2025. Influence of the airflow concept on the aerosol spreading in a generic train compartment. In: Transport Transitions: Advancing Sustainable and Inclusive Mobility. Springer Nature Switzerland, pp. 410–416. http://dx.doi.org/10.1007/978-3-031-88974-5_60.

Schmeling, D., Kühn, M., Schiepel, D., Dannhauer, A., Lange, P., Kohl, A., Niehaus, K., Berlitz, T., Jäckle, M., Kwitschinski, T., Tielkes, T., 2022. Analysis of aerosol spreading in a German Inter City Express (ICE) train carriage. Build. Environ. 222, 109363. http://dx.doi.org/10.1016/j.buildenv.2022.109363.

Schmeling, D., Shishkin, A., 2025. Healthier passenger rail: Influence of the recirculation system on the spreading ofexhaled particles in a passenger train. In: Proceedings of the WCRR2025, Colorado Springs, USA. https://elib.dlr.de/206638/.

Schmeling, D., Shishkin, A., Schiepel, D., Wagner, C., 2023. Numerical and experimental study of aerosol dispersion in the Do728 aircraft cabin. CEAS Aeronaut. J. 14 (2), 509–526. http://dx.doi.org/10.1007/s13272-023-00644-3.

Sensirion AG, 2019. Mechanical Design and Assembly Guidelines for SPS30 - Particulate Matter Sensor. Online. URL https://sensirion.com/media/documents/7990F04A/616544B0/Sensirion_Particulate_Matter_AppNotes_SPS30_Mechanical_Design_and_As.pdf.(accessed 30 June 2026).

Sensirion AG, 2020. Sensor Specification Statement - How to Understand Specifications of Sensirion Particulate Matter Sensors. Online. URL https://sensirion.com/media/documents/B7AAA101/61653FB8/Sensirion_Particulate_Matter_AppNotes_Specification_Statement.pdf.(accessed 30 June 2026).

Songbo, W., Tian, L., Jiye, Z., 2025. Study on air quality improvement in train compartments by coordinated exhaust of multiple air outlets. Railw. Eng. Sci. http://dx.doi.org/10.1007/s40534-025-00398-0.

Tu, M., Olofsson, U., 2024. Estimating PM levels on an underground metro platform by exploring a new model-based factor research. Atmospheric Environ.: X 22, 100261. http://dx.doi.org/10.1016/j.aeaoa.2024.100261.

Wang, H., Lin, M., Chen, Y., 2014. Performance evaluation of air distribution systems in three different China railway high-speed train cabins using numerical simulation. Build. Simul. 7 (6), 629–638. http://dx.doi.org/10.1007/s12273-014-0168-5.

Webner, F., Shishkin, A., Schmeling, D., Wagner, C., 2024. A direct infection risk model for CFD predictions and its application to SARS-CoV-2 aircraft cabin transmission. Indoor Air 2024 (1), http://dx.doi.org/10.1155/2024/9927275.

World Health Organization (WHO), 2021. Coronavirus disease (COVID-19): How is it transmitted?. Online. https://www.who.int/news-room/questions-and-answers/item/coronavirus-disease-covid-19-how-is-it-transmitted. (accessed 24 April 2026).

Wu, F., Yu, C., Xu, R., Li, H., Yu, J., Zhou, S., 2024. Risk evaluation of respiratory droplet dispersion in high-speed train compartments with different air circulation systems. Atmospheric Pollut. Res. 15 (9), 102197. http://dx.doi.org/10.1016/j.apr.2024.102197.

Xu, R., Qian, B., Wu, F., Li, X., Zhang, G., Wang, L., 2022. Dispersion of evaporating droplets in the passenger compartment of high-speed train. J. Build. Eng. 48, 104001. http://dx.doi.org/10.1016/j.jobe.2022.104001.